MICROSCOPY

Microscopy, 2019, 254–260
doi: 10.1093/jmicro/dfz007
Advance Access Publication Date: 12 March 2019

Article

Electron holography on Fraunhofer diffraction

Ken Harada[1,2,*], Kodai Niitsu[3], Keiko Shimada[1], Tetsuji Kodama[4], Tetsuya Akashi[5,6], Yoshimasa A. Ono[1], Daisuke Shindo[1,7], Hiroyuki Shinada[5], and Shigeo Mori[2]

[1]CEMS, RIKEN (The Institute of Physical and Chemical Research), Hatoyama, Saitama 350-0395, Japan, [2]Department of Materials Science, Osaka Prefecture University, Sakai, Osaka 599-8531, Japan, [3]Department of Materials Science & Engineering, Kyoto University, Kyoto, Kyoto 606-8501, Japan, [4]Graduate School of Science and Technology, Meijo University, Nagoya, Aichi 468-8502, Japan, [5]Research & Development Group, Hitachi, Ltd., Hatoyama, Saitama 350-0395, Japan, [6]Department of Applied Quantum Physics and Nuclear Engineering, Kyushu University, Fukuoka, Fukuoka 810-0395, Japan, and [7]Institute of Multidisciplinary Research for Advanced Materials (IMRAM), Tohoku University, Sendai, Miyagi 980-8577, Japan

[*]To whom correspondence should be addressed. E-mail: kharada@riken.jp

Received 14 November 2018; Editorial Decision 28 January 2019; Accepted 30 January 2019

Abstract

Electron holography in Fraunhofer region was realized by using an asymmetric double slit. A Fraunhofer diffraction wave from a wider slit worked as an objective wave interfered with a plane wave from a narrower slit as a reference wave under the pre-Fraunhofer condition and recorded as a hologram. Here, the pre-Fraunhofer condition means that the following conditions are simultaneously satisfied: single-slit observations are performed under the Fraunhofer condition and the double-slit observations are performed under the Fresnel condition. Amplitude and phase distributions of the Fraunhofer diffraction wave were reconstructed from the hologram by the Fourier transform reconstruction method. The reconstructed amplitude and phase images corresponded to Fraunhofer diffraction patterns; in particular, the phase steps of π at each band pattern in the phase image were confirmed. We hope that the developed Fraunhofer electron holography can be extended to a direct phase detection method in the reciprocal space.

Key words: electron holography, Fraunhofer diffraction, double slit, phase distribution, interferometry

Introduction

Recently several electron imaging methods have been developed by utilizing not only the real space but also the reciprocal space, such as diffractive imaging [1–3] and ptychography [4–6]. These developments are due to advancement of the following technologies: highly sensitive imaging technologies based on direct electron detection cameras [7], image-processing technologies for multiple and large-scale image data [8], and iteration algorisms for image data analysis [9,10]. Understanding of wave propagation between the real space and the reciprocal space is very important from the optical point of view, especially in

image reconstructions in the real space from data in the reciprocal space, and in phase retrieval for data in the real and reciprocal spaces. Precise investigation of amplitude and phase distributions of wave fields in the reciprocal space is necessary for these purposes. In wave optics, this has already been performed theoretically as well as experimentally [11,12].

In electron microscopy, the amplitude and phase distributions of wave fields in the reciprocal space, such as diffraction planes, have been extensively discussed in phase microscopy [13,14] and vortex beam microscopy [15–19]. In particular, the phase distribution in the reciprocal space is difficult to detect directly even by using holography technique because intensity of the object wave in diffraction patterns is a few orders of magnitudes larger than that of the diffracted waves and also because no appropriate reference waves exist in the reciprocal space. Few trials using electron microscopes have been reported except for electron holography approach for vortex beams [18,19]. In light optics, on the other hand, several experimental and theoretical studies have been performed using microwaves on the wave fields in the reciprocal space, i.e. in the back focal planes [12,20,21].

In this paper, we propose electron holography on Fraunhofer diffraction utilizing an asymmetric double slit created by a biprism from a symmetric double slit placed at the specimen position [22]. A Fraunhofer diffraction wave from a wider slit can work as an objective wave interfering with a plane-wave-like wave from an extremely narrower slit acting as a reference wave. The Fraunhofer diffraction wave was used successfully to record holograms and to reconstruct amplitude and phase distributions from the hologram through the Fourier transform reconstruction method. The reconstructed phase profile had phase steps of π at each band pattern in the phase images. These results are consistent with those of microwave data [12,20,21], indicating that electron beams were diffracted and propagated as plane waves.

Theoretical

Figure 1 shows an illustration for explaining the concept of this study and 'pre-Fraunhofer condition' [22]. An asymmetric double-slit, which has one narrow opening and other slightly wider opening, is positioned at the upstream of a coherent electron wave. In the downstream side, two waves pass through the slit-openings and their propagations are illustrated. The term 'pre-Fraunhofer condition' indicates that the following conditions are simultaneously satisfied: each single-slit observations are performed under the Fraunhofer condition and the double-slit observations are performed under the Fresnel condition. In general, Fraunhofer/Fresnel conditions depend on wavelengths, sizes of the scattering objects, and propagation distances. When two scattering objects with different sizes are observed under appropriate conditions regarding the wavelength and the propagation distance, the following observation condition is possible: the Fraunhofer condition is realized for a smaller object and the Fresnel condition is realized for a larger object at the same time under a single experimental condition. In the present paper, an asymmetric double slit was used as shown in Figs 1 and 2, and the propagation distance was chosen for the Fraunhofer condition for each slit with the opening width as a parameter and the propagation distance was chosen for the Fresnel condition for the double slit with widths of the slit spacing as a parameter. To describe this experimental condition we coined the term 'pre-Fraunhofer condition'.

Fresnel fringes from the edges of the either opening or interference fringes due to the two passed waves were numerically obtained using Fresnel diffraction theory [11] in the wave optics. Since the Fraunhofer diffraction can be analyzed by the Fresnel diffraction theory as a case of an extremely large-distance propagation, two waves $\phi_{\mathrm{right}}(x,\ \Delta f)$ and $\phi_{\mathrm{left}}(x,\ \Delta f)$ can be written as follows:

$$\begin{aligned}\phi_{\mathrm{right}}(x,\ \Delta f) &= \sqrt{\frac{\lambda\Delta f}{2}}\int_{\alpha_{\mathrm{right1}}}^{\alpha_{\mathrm{right2}}}\exp\frac{i\pi\alpha(x,\ \Delta f)^2}{2}\mathrm{d}\alpha \\ &= \sqrt{\frac{\lambda\Delta f}{2}}\int_{\alpha_{\mathrm{right1}}}^{\alpha_{\mathrm{right2}}}\left(\cos\frac{\pi\alpha(x,\ \Delta f)^2}{2}\right. \\ &\quad \left.+\, i\sin\frac{\pi\alpha(x,\ \Delta f)^2}{2}\right)d\alpha \\ &= \sqrt{\frac{\lambda\Delta f}{2}}\{[C(\alpha_{\mathrm{right2}}(x,\ \Delta f)) - C(\alpha_{\mathrm{right1}}(\mathrm{x},\Delta f))] \\ &\quad + i[S(\alpha_{\mathrm{right2}}(x,\ \Delta f)) \\ &\quad - S(\alpha_{\mathrm{right1}}(x,\ \Delta f))]\}\end{aligned} \tag{1}$$

$$\begin{aligned}\phi_{\mathrm{left}}(x,\ \Delta f) &= \sqrt{\frac{\lambda\Delta f}{2}}\int_{\alpha_{\mathrm{left1}}}^{\alpha_{\mathrm{left2}}}\exp\frac{i\pi\alpha(x,\ \Delta f)^2}{2}\mathrm{d}\alpha \\ &= \sqrt{\frac{\lambda\Delta f}{2}}\int_{\alpha_{\mathrm{left1}}}^{\alpha_{\mathrm{left2}}}\left(\cos\frac{\pi\alpha(x,\ \Delta f)^2}{2} + i\sin\frac{\pi\alpha(x,\ \Delta f)^2}{2}\right)\mathrm{d}\alpha \\ &= \sqrt{\frac{\lambda\Delta f}{2}}\{[C(\alpha_{\mathrm{left2}}(x,\ \Delta f)) - C(\alpha_{\mathrm{left1}}(x,\ \Delta f))] \\ &\quad + i[S(\alpha_{\mathrm{left2}}(x,\ \Delta f)) - S(\alpha_{\mathrm{left1}}(x,\ \Delta f))]\},\end{aligned} \tag{2}$$

where $\phi_{\mathrm{right}}(x,\ \Delta f)$ and $\phi_{\mathrm{left}}(x,\ \Delta f)$ are complex amplitude distributions of the waves projected on the observation plane from the right and left slits, respectively. In addition, x indicates the coordinate of the observation plane whose origin is the midpoint of the projected image of the double slit on the observation plane; Δf is the propagation distance between the slit plane and the observation plane, i.e.

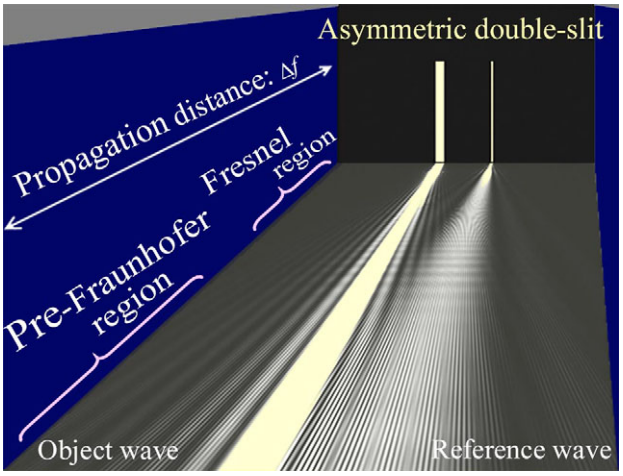

Fig. 1. Illustration of the present experimental setup and for explanation of 'pre-Fraunhofer condition.' An electron wave passed through the left single slit is an object wave and an electron wave passed through the right narrower slit is a reference wave. In the pre-Fraunhofer region, the reference wave spreads to an almost plane-wave-like wave enabling to record holograms of the Fraunhofer diffraction pattern on the left.

the defocus distance; $\alpha(x,\ \Delta f)$ is a function of x and Δf denoting a conventional variable of the Fresnel integration derived from the geometrical ray-path from the slit plane to the observation plane; λ is the wavelength; and $C(\alpha,\ \Delta f)$ and $S(\alpha,\ \Delta f)$ denote Fresnel integrals in Cosine-type and Sine-type, respectively. When the slit widths are ω_{right} and ω_{left} and spacing between the slits is d, then the variables of Fresnel integrations, α_{right1}, α_{right2}, α_{left1} and α_{left2}, are given by [11],

$$\alpha_{\text{right1}}(x,\ \Delta f) = \sqrt{\frac{2}{\lambda\Delta f}}\left(\frac{d}{2} + \frac{\omega_{\text{right}}}{2} - x\right), \tag{3}$$

$$\alpha_{\text{right2}}(x,\ \Delta f) = \sqrt{\frac{2}{\lambda\Delta f}}\left(\frac{d}{2} - \frac{\omega_{\text{right}}}{2} - x\right), \tag{4}$$

$$\alpha_{\text{left1}}(x,\ \Delta f) = \sqrt{\frac{2}{\lambda\Delta f}}\left(-\frac{d}{2} - \frac{\omega_{\text{left}}}{2} - x\right), \tag{5}$$

$$\alpha_{\text{left2}}(x,\ \Delta f) = \sqrt{\frac{2}{\lambda\Delta f}}\left(-\frac{d}{2} + \frac{\omega_{\text{left}}}{2} - x\right). \tag{6}$$

Using the above equations, we obtain a normalized intensity distribution on the objective plane $I_{\text{norm}}(x,\ \Delta f)$ with the two wave interference patterns,

$$\begin{aligned} I_{\text{norm}}(x,\ \Delta f) &= \frac{1}{I_{0right} + I_{0left}} \times |\phi_{\text{right}}(x,\ \Delta f) + \phi_{\text{left}}(x,\ \Delta f)|^2 \\ &= \frac{1}{I_{0right} + I_{0left}} \times \{[C(\alpha_{\text{right2}}(x,\ \Delta f)) - C(\alpha_{\text{right1}}(x,\ \Delta f))]^2, \\ &\quad + C(\alpha_{\text{left2}}(x,\ \Delta f)) - C(\alpha_{\text{left1}}(x,\ \Delta f))]^2 \\ &\quad + [S(\alpha_{\text{right2}}(x,\ \Delta f)) - S(\alpha_{\text{right1}}(x,\ \Delta f)) \\ &\quad + S(\alpha_{\text{left2}}(x,\ \Delta f)) - S(\alpha_{\text{left1}}(x,\ \Delta f))]^2\} \end{aligned} \tag{7}$$

where $I_{0\text{right}}$ and $I_{0\text{left}}$ are the intensities generated by the waves from each single slit at the optical axis on the observation plane, $x = 0$. In the Fresnel diffraction theory, Eq. 7 describes not only the interference of two waves on the observation plane but also the propagation process as a function of Δf.

Figure 2 shows the calculated propagation behavior of two waves passed through the asymmetric double slit when the right slit width is varied from 5 to 38 nm, which are the same as those of the experiments: (a) 38 nm, (b) 22 nm, (c) 10 nm and (d) 5 nm. Other parameters in the calculation are also chosen to be the same as those in the experiments: $\omega_{\text{left}} = 120$ nm, $d = 800$ nm, and $\lambda = 0.76$ pm for 1.2-MeV electron beams. The yellow horizontal lines indicate the position of the observation plane for $\Delta f = 23.2$ mm.

Although the right-slit width of 5 nm is four orders of magnitude larger than the wavelength λ, the electron waves passed through the right slit spread out quickly just like a plane wave and overlaps with the electron wave passed through the left slit (see, Fig. 2d). Because of this behavior, we conjecture that waves passed through the narrower slit with less than several nm wide can be used as a reference wave against the other wave passed through a much wider slit under the Fraunhofer condition. In this way, electron holography under the Fraunhofer diffraction condition can be realized.

Experimental

In the present double-slit experiments, a 1.2 MV field-emission transmission electron microscope [23] with the wavelength of 0.76 pm was used because the microscope can generate highly coherent electron beams whose coherence length is more than 95 μm [24]. Figure 3 shows a schematic diagram of the optical system for the double-slit experiment. A symmetric double slit was installed at the specimen position. The first image of the double slit was formed just on the biprism (BP) filament, where a conjugate relation between the slit and the filament was realized. This filament (1.6 μm in diameter) made of a quartz fiber with Pt-Pd coating was utilized to control the opening

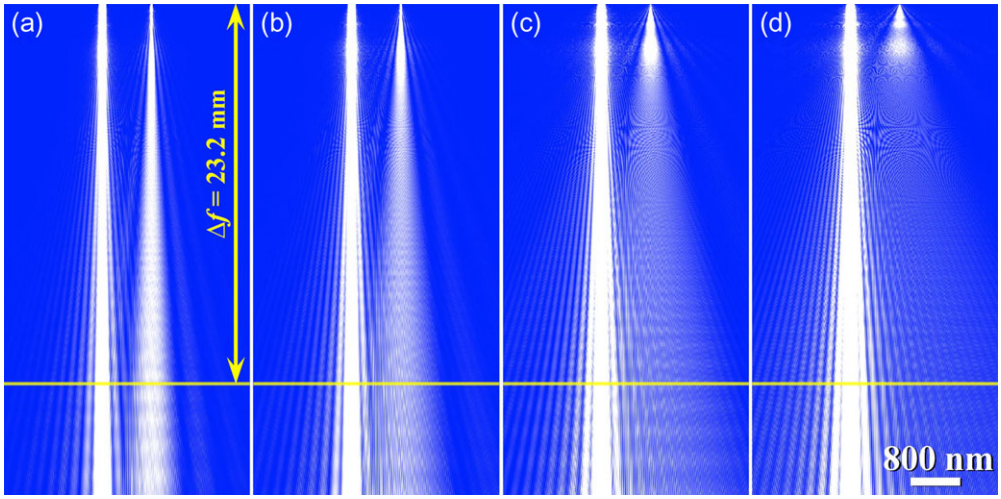

Fig. 2. Wave optical simulation on wave propagation from an asymmetric double slit by changing the right-slit width ω_{right}: (a) 38 nm, (b) 22 nm, (c) 10 nm, and (d) 5 nm. The left-slit width ω_{left} is 120 nm.

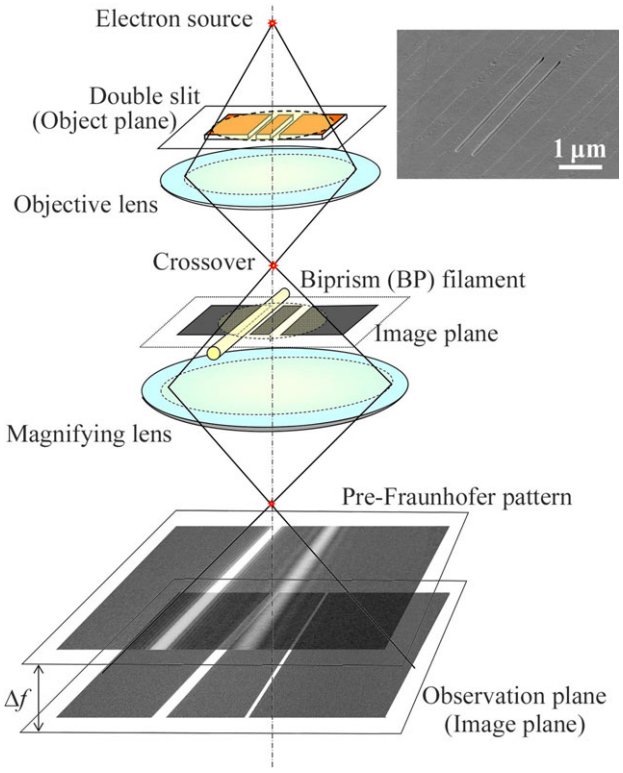

Fig. 3. A schematic diagram of the optical system. A double slit is installed at the specimen position and is imaged on the electron biprism (BP) filaments. The double slit and the BP filament are focused on the image plane. Defocusing conditions are controlled by the magnifying lens below the objective lens. The width of the right slit is varied by using the BP filament. In the inset is a scanning electron micrograph of the fabricated double slit, having 120 nm width, 10 μm length and 800 nm spacing between the slit.

width of the right slit. The defocused image patterns formed by using the magnifying lens varied from the infocus condition to the Fresnel condition, and to the Fraunhofer condition. Since a crossover of the incident electron beam as the electron source was formed above the double slit, an under-focus condition for the defocusing was adopted, and defocused image patterns were enlarged by using successive magnifying lenses. The reason for choosing under-focus condition in this experiment was that the crossover was located above the specimen in this optical system. The defocusing operation deviates the infocus point and moves it close to the crossover (see, Fig. 3), generating large defocusing.

The double slits with two rectangle openings having 120 nm width, 10 μm length, and 800 nm spacing between the slits were made of copper foil of 1 μm thick by using an FIB instrument (NB-5000, Hitachi High-Technologies Corp.). The inset in Fig. 3 shows a scanning electron micrograph of the fabricated double slit. Advanced direct electron detection camera system (3711 × 3839 pixels, K2®Summit Camera, Gatan, Inc.) installed in the microscope was used.

Results and discussion

Figure 4 shows series of varied patterns depending on the right slit width: (a) 38 nm, (b) 22 nm, (c) 10 nm and (d) 5 nm. The defocus distance Δf, indicating the propagation distance from the slit plane to observation plane, was 23.2 mm. Blue inset images at the bottom of each panel are calculated results in Fig. 2. The calculated images of both Fresnel fringes and interference fringes are in good agreement with the experimental interferograms. This indicates that electrons passed through both slits as waves and interfered with each other on the observation plane. Furthermore, the direct wave (central maximum wave) from the right slit (smaller slit) spreads widely with a level to be considered as a background and was superimposed

on the Fraunhofer diffraction wave from the left slit (larger slit): consequently, the intensity of the direct wave is difficult to recognize. Since the diffraction wave from the right slit can be regarded as an almost plane-wave-like wave, this wave can be used as a reference wave in holography, and then Fraunhofer hologram of the left slit is recorded. This behavior is also shown theoretically in Fig. 2d.

The size and contrast of the Fresnel fringes for the right narrower slit greatly varied and depended on the slit width, whereas the spacing of the interference fringes did not depend on the right slit width. Since spacing of the interference fringes mostly depended on the distance of the two slits d (= 800 nm), the spacing of the interference fringes was kept at about 22 nm during the experiment.

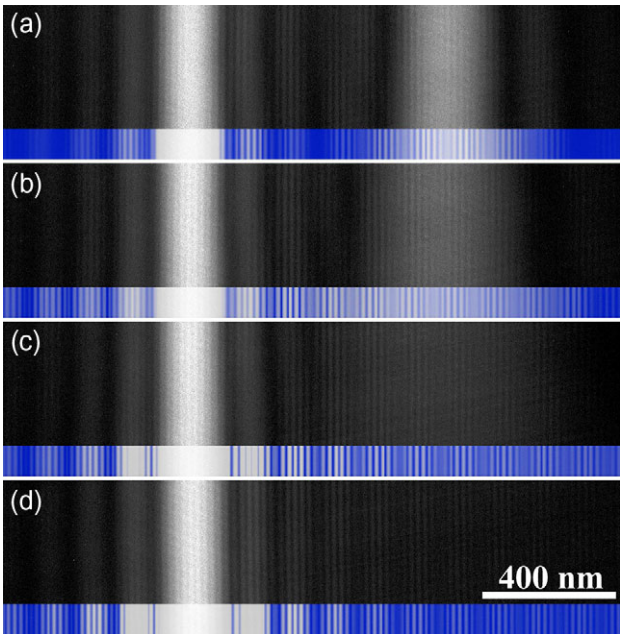

Fig. 4. Series of the experimental results by changing the right slit width ω_{right}: (a) ω_{right} = 38 nm, (b) 22 nm, (c) 10 nm and (d) 5 nm. The defocus distance Δf was 23.2 mm for all panels. Inset images in blue at the bottom of each panel are calculated results along the yellow lines in Fig. 2.

Figure 5a shows an electron hologram of a Fraunhofer diffraction from the left slit with 120 nm width at the defocus distance Δf of 23.2 mm; here the electron wave passed through the right slit with 5 nm width was used as the reference wave. Figure 5b shows a Fraunhofer diffraction pattern from the left slit alone with the right slit closed. As is clearly shown in these micrographs, uniform and homogeneous Fraunhofer diffraction patterns were obtained over a wide area of a few micrometers. Comparison of Figs 5a and b indicates that only interference fringes due to the two-wave interference disappeared in (b) and that the opening/closing of the right slit does not affect the Fraunhofer diffraction pattern from the left slit. In other words, Fig. 5 is an experimental proof that shows that the reference wave from right slit works as a plane wave at the observation plane with defocusing Δf = 23.2 mm. Then, the conventional electron holography reconstruction technique, Fourier transform method can be adopted to reconstruct the hologram in Fig. 5a.

Since the electron holography on the Fraunhofer diffraction is recorded and reconstructed in a region which is neither a real space nor a reciprocal space, the definition of the scale of the image becomes ambiguous. In Figs 5 and 6, the scale bar was given based on the projected size from the object plane to the observation plane (see, Fig. 2).

Figure 6 shows reconstructed amplitude and phase distributions of the Fraunhofer diffraction pattern in the white square region in Fig. 5a. For reconstruction, a conventional Fourier transform was used. The amplitude

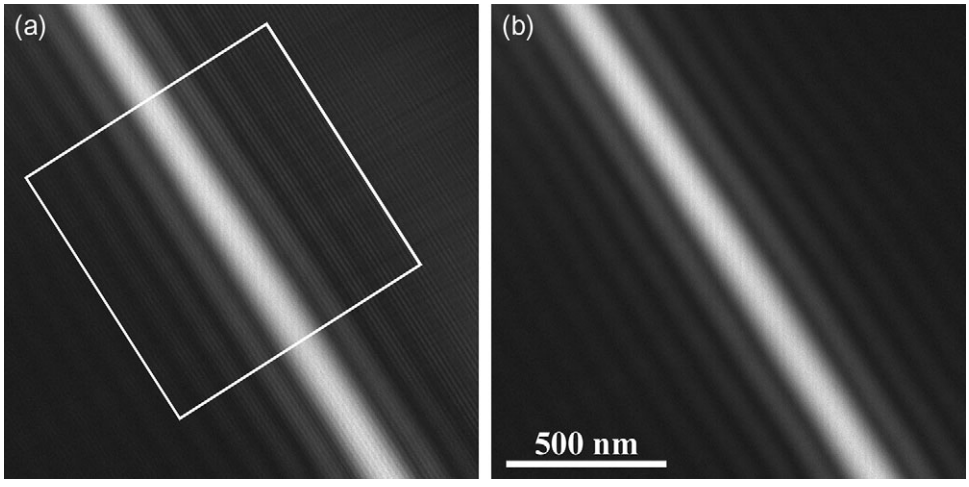

Fig. 5. (a) Electron hologram of a Fraunhofer diffraction from the left slit. (b) The Fraunhofer diffraction pattern only from the left slit with 120 nm width recorded at the defocus distance Δf of 23.2 mm. Amplitude and phase distributions in a white square region in (a) are reconstructed and shown in Fig. 6.

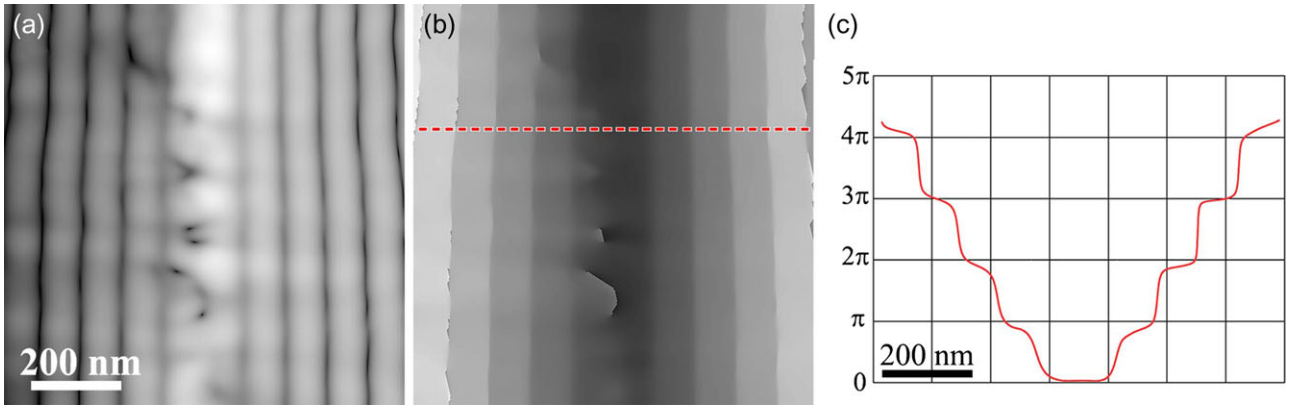

Fig. 6. Reconstructed amplitude and phase images, and phase profile; (a) amplitude image, (b) phase image, and (c) phase profile along the red broken line in (b). Fringe interval in the Fraunhofer pattern becomes slightly narrower at the top of the panel, probably caused by the wider opening width of the left slit. The amount width increment is estimated to be about 7 nm, which is attributed to fluctuations in the film thickness. Non-uniform patterns in the reconstructed center band in (a) and (b) are artifacts probably due to a loss of interference fringes of the hologram; however, these patterns have no direct effects on experimental results.

image corresponds to the Fraunhofer diffraction pattern in the reciprocal space generated by a single slit. The phase distribution shows a band-shape feature. The phase profile along the red broken line in Fig. 6b is given in Fig. 6c, showing a step-like phase profile with π difference between steps. It can be explained that the amplitude distribution of the Fraunhofer diffraction of the rectangular opening is represented by the sinc function. When the alternating change of the positive/negative values of the amplitude distribution is stacked as a π step of the phase, the phase distribution is represented in steps of π for each Fraunhofer fringe of the slit. These observed phase steps are similar to those of microwaves at the back focal plane of an imaging lens reported in the 1950s [12,20,21]. These results show that incompletely shielded electrons of less than 2.7% of the incident electrons estimated using multi-slice simulation did not affect the interferometry.

These observations lead us to believe that the interferometry developed in the present study, named as Fraunhofer electron holography, can be widely applied to amplitude and phase distribution studies in many kinds of materials, for example magnetic materials, dielectric materials, and functional materials, by placing their specimens at the left slit position.

Conclusion

We realized electron holography in the reciprocal space named as Fraunhofer electron holography by using an asymmetric double slit. A Fraunhofer diffraction wave from the wider slit as an object wave was interfered with a plane wave from another narrower slit as a reference wave, and was recorded as Fraunhofer hologram. When reconstructed, a Fraunhofer diffraction wave had the phase step of π, which is consistent with the results of the Fraunhofer diffraction patterns in microwave studies in 1950s. We believe the developed interferometry, Fraunhofer electron holography, will be used widely as a new electron holography technique for analyzing electro-magnetic materials, such as electron vortex beams.

Acknowledgments

Authors would like to thank Dr Y. Takahashi at Hitachi Research and Development Group for the multi-slice simulation and Dr H. Yoshikawa at NIMS for his valuable discussion about the electron-material interactions. Authors also would like to acknowledge Mr N. Moriya at Hitachi Research and Development Group with his technical support.

Funding

This work was supported by JSPS KAKENHI (Grant-in-Aid for Scientific Research), Grant Number (B)18H03475.

References

1. Miao J, Charalambous P, Kirz J, and Sayer D (1999) Extending the methodology of X-ray crystallography to allow imaging of micrometre-sized non-crystalline specimens. *Nature* 400: 342–344.
2. Kamimura O, Kawahara K, Doi T, Dobashi T, Abe T, and Gohara K (2008) Diffraction microscopy using 20 kV electron beam for multiwall carbon nanotubes. *Appl. Phys. Lett.* 92: 024106 1–3.
3. Morishita S, Yamasaki J, Nakamura K, Kato T, and Tanaka N (2008) Diffractive imaging of the dumbbell structure in silicon by spherical-aberration-corrected electron diffraction. *Appl. Phys. Lett.* 93: 183103 1–3.
4. Rodenburg J M, Hurst A C, and Cullis A G (2007) Transmission microscopy without lenses for objects of unlimited size. *Ultramicroscopy* 107: 227–231.

5. Lupini A R, Oxley M P, and Kalinin S V (2016) Pushing the limits of electron ptychography. *Science* 362: 399–400.
6. Jiang Y, Chen Z, Han Y, Deb P, Gao H, Xie S, Ourohit P, Tate M W, Park J, Gruner S M, Elser V, and Muller D A (2018) Electron ptychography of 2D materials to deep sub-ångström resolution. *Nature* 559: 343–358.
7. McMullan G, Faruqi A R, Clare D, and Henderson R (2014) Comparison of optimal performance at 300 keV of three direct electron detectors for use in low dose electron microscopy. *Ultramicroscopy* 147: 156–163.
8. Muto S, Rusz J, Tatsumi K, Adam R, Arai S, Kocevski V, Oppeneer P M, Bürgler D E, and Schneider C M (2014) Quantitative characterization of nanoscale polycrystalline magnets with electron magnetic circular dichroism. *Nat. Comm.* 5: 1–7.
9. Allen L J, McBride W, O'Leary N L, and Oxley M P (2004) Exit wave reconstruction at atomic resolution. *Ultramicroscopy* 100: 91–104.
10. Tamura T, Nakane Y, Nakajima H, Mori S, Harada K, and Takai Y (2018) Phase retrieval using through-focus images in Lorentz transmission electron microscopy. *Microscopy* 67: 171–177.
11. Born M, and Wolf E (Pergamon Press, 1985) Principles of Optics, 6th ed. Ch 8, 428–435.
12. Linfoot E H, and Wolf E (1956) Phase distribution near focus in an aberration-free diffraction image. *Proc. Phys. Soc. B* 69: 823–832.
13. Malac M, Beleggia M, Kawasaki M, Li P, and Egerton R F (2012) Convenient contrast enhancement by a hole-free phase plate. *Ultramicroscopy* 118: 77–89.
14. Kotani A, Harada K, Malac M, Salomons M, Hayashida M, and Mori S (2018) Observation of FeGe skyrmions by electron phase microscopy with hole-free phase plate. *AIP Adv.* 8: 055216 1–7.
15. McMorran B J, Agrawal A, Anderson I M, Herzing A A, Lezec H J, McClelland J J, and Unguris J (2011) Electron vortex beams with high quanta of orbital angular momentum. *Science* 331: 192–195.
16. Saitoh K, Hasegawa Y, Hirakawa K, Tanaka N, and Uchida M (2013) Measureing the orbital angular momentum of electron vortex beams using a fork grating. *Phys. Rev. Lett.* 111: 074801 1–5.
17. Harada K, Niitsu K, Shimada K, Ono Y A, and Shindo D (2017) Measurement of vortex beam phases by electron holography. *Micopsc. Microanal.* 23: 588–589.
18. McMorran B J, Agrawal A, Ercius P A, Grillo V, Herzing A A, Harvey T R, Linck M, and Pierce J S (2017) Origin and demonstrations of electrons with orbital angular momentum. *Phil. Trans. R. Soc. A* 375: 20150434 1–18.
19. Harada K, Shimada K, Ono Y A, Iwasaki Y, Niitsu K, and Shindo D (2018) Electron holography study on vortex beam phases in real space. *Micopsc. Microanal.* 24: 1470–1471.
20. Farnell G W (1957) Calculated intensity and phase distrubution in the image space of a microwave lens. *Can. J. Phys.* 35: 777–783.
21. Farnell G W (1958) Measured phase distribution in the image space of a microwave lens. *Can. J. Phys.* 36: 935–943.
22. Harada K, Akashi T, Niitsu K, Shimada K, Ono Y A, Shindo D, Shinada H, and Mori S (2018) Interference experiment with asymmetric double slit by using 1.2-MV field emission transmission electron microscope. *Sic. Rep.* 8: 1008 1–10.
23. Akashi T, Takahashi Y, Tanigaki T, Shimakura T, Kawasaki T, Furutsu T, Shinada H, Müller H, Haider M, Osakabe N, and Tonomura A (2015) Aberration corrected 1.2-MV cold field emission transmission electron microscope with a sub-50-pm resolution. *Appl. Phys. Lett.* 106: 074101 1–4.
24. Akashi T, Takahashi Y, Harada K, Onai T, Ono Y A, Shinada H, and Murakami Y (2018) Illumination semiangle of 10^{-9} rad achieved in a 1.2-MV atomic resolution holography transmission electron microscope. *Microscopy* 67: 286–290.